Time-lapse AVO inversion: Application to synthetic data

A. Nassir Saeed, Laurence R. Lines, and Gary F. Margrave

ABSTRACT

A reservoir characterization workflow for time-lapse studies requires integrating seismic data of different vintages and well logs information into a single consistent model to delineate changes of reservoir parameters.

In this study, we implemented three different time-lapse AVO inversion algorithms (*total inversion of the differences, inversion of seismic difference only* and *sequential reflectivity-constrained inversion*) using synthetic data that simulate a time-lapse model of a heavy oil reservoir. Elastic physical parameters of the time-lapse model were chosen to represent reservoir conditions at pre-production and post-production periods after reservoir depletion.

The time-lapse AVO inversion schemes simultaneously invert baseline and monitor seismic data to estimate the change of model parameters. The proposed algorithms have proved their robustness in terms of computation time as well as stability in presence of noise to ensure smooth changes in estimating reservoir attributes from time-lapse inversion.

INTRODUCTION

In time-lapse AVO inversion, we seek to estimate elastic parameters changes for baseline and monitor seismic surveys of a hydrocarbon reservoir after depletion. Successful estimation of these elastic differences can further assist in delineation of fluid saturation and pressure changes (LandrØ, 2001) in the reservoir due to production processes.

A time-lapse model (Saeed et al., 2010a) that simulates a heavy oil reservoir of Pikes Peak oil field is used in this study. Synthetic data were generated using Syngram software developed by CREWES. Figures (1 and 2) are for P-P synthetic data of baseline and monitoring models respectively, while figures (3 and 4) represent P-S synthetic data of the baseline and monitoring models.

TIME-LAPSE AVO INVERSION

Practical inversion techniques that simultaneously invert seismic data of different vintages (Saeed et al., 2011) are used in this study. The objectives from proposed inverse techniques are to improve model parameters estimations in the presence of noise, and proposed algorithms have proved their robustness in terms of accuracy and computation time.

For two given data sets, says (base, $\mathbf{d_0}$, and a monitor, $\mathbf{d_1}$,), reflectivity data can be written as:

$$d_0 = G_0\, m_0 \quad \text{for base line} \tag{1}$$

$$d_1 = G_1\, m_1 \quad \text{for monitor line} \tag{2}$$

where,

d is seismic data, **G** is forward operator, and **m** is unknown model parameters sought.

The least-squares inverse problems of time-lapse seismic surveys requires minimization of cost functions below

$$J(m_0) = \|\boldsymbol{G_0 m_0 - d_0}\|^2 + \lambda^2 \|\boldsymbol{G_0 m_0}\|^2 \tag{3}$$

$$J(m_1) = \|\boldsymbol{G_1 m_1 - d_1}\|^2 + \lambda^2 \|\boldsymbol{G_1 m_1}\|^2 \tag{4}$$

which give the solutions

$$m_0 = (\boldsymbol{G_0^T} G_0 + \lambda^2 \boldsymbol{R_0^T} R_0)^{-1} \boldsymbol{G_0^T d_0} \tag{5}$$

$$\mathrm{m_1} = (\mathrm{G_1^T G_1} + \lambda^2 \mathrm{R_1^T R_1})^{-1} \mathrm{G_1^T d_1} \tag{6}$$

where,

R and **λ** are the regularization operator and parameter (Constable et al., 1987) respectively.

The low frequency component of well logs is then added to model parameters using the BLIMP module (Ferguson and Margrave, 1996). The estimated model parameters ($\mathbf{m_0}$ and $\mathbf{m_1}$) resulting for inverting seismic data vintages separately are then manipulated to be either as differences between estimated base and monitor model parameters ($\mathbf{\Delta m = m_1 - m_0}$) or as percentage of changes between base and monitoring model parameters ($\boldsymbol{\Omega_{m\%} = \frac{\Delta m}{m_0}.100}$).

In the following sections, we present applications of three different time-lapse AVO inversion schemes (total inversion of the differences, inversion of seismic differences only and sequential reflectivity-constrained inversion) simultaneously invert baseline and monitor seismic data to estimate the change of model parameters. The obtained model parameters can also be presented as percentage of changes.

Total inversion of differences

The total inversion of differences to estimate model parameters change of time-lapse data is carried out by simultaneously inverting baseline and monitor data. Thus, equations (1 and 2) are then re-arranged as

$$G_1\, m_1 - G_0\, m_0 = d_1 - d_0 \tag{7}$$

By using ($\mathbf{\Delta G = G_1 - G_0}$), and substituting for $\mathbf{G_1}$in equation (7), the time-lapse AVO inversion for estimating model parameters of monitor line ($\boldsymbol{m_1}$) and model parameter changes ($\boldsymbol{\Delta m}$) requires that equation (7) to be written as:

$$(\Delta G + G_0)\, m_1 - G_0\, m_0 = \Delta d \tag{8}$$

Re-arranging (8), yields

$$\Delta G m_1 + G_0 \Delta m = \Delta d \tag{9}$$

In augmented matrix notation, cost functions (3 and 4) can be jointly- inverted, and written as:

$$J(\boldsymbol{m_1}, \boldsymbol{\Delta m}) = \left\| \begin{bmatrix} \Delta \mathbf{G} & \mathbf{0} \\ \mathbf{0} & \boldsymbol{G_0} \end{bmatrix} \begin{bmatrix} \boldsymbol{m_1} \\ \Delta \mathbf{m} \end{bmatrix} - \begin{bmatrix} \boldsymbol{d_1} \\ \boldsymbol{d_0} \end{bmatrix} \right\|^2 + \begin{bmatrix} \lambda^2 \boldsymbol{R_1^T R_1} & \mathbf{0} \\ \mathbf{0} & \lambda^2 \boldsymbol{R_0^T} R_0 \end{bmatrix} \begin{bmatrix} \boldsymbol{m_1} \\ \Delta \mathbf{m} \end{bmatrix} \tag{10}$$

Since the outputs from equation (10) are $\mathbf{m_1}$ and $\mathbf{\Delta m}$ respectively, then model parameters for the base model can also be estimated as:

$$\mathbf{m_0} = \mathbf{m_1} - \mathbf{\Delta m} \tag{11}$$

Figures (5 and 6) are inverted to obtain model parameters ($\frac{\Delta \mathbf{I}}{\mathbf{I}}$, $\frac{\Delta \mathbf{J}}{\mathbf{J}}$ and $\frac{\Delta \boldsymbol{\rho}}{\boldsymbol{\rho}}$) for monitor model and model parameters changes [$\Delta(\frac{\Delta \mathbf{I}}{\mathbf{I}})$, $\Delta(\frac{\Delta \mathbf{J}}{\mathbf{J}})$ and $\Delta(\frac{\Delta \boldsymbol{\rho}}{\boldsymbol{\rho}})$] for the time-lapse survey before adding low frequency component from well logs. Figure (7) shows estimated model parameters ($\frac{\Delta \mathbf{I}}{\mathbf{I}}$, $\frac{\Delta \mathbf{J}}{\mathbf{J}}$ and $\frac{\Delta \boldsymbol{\rho}}{\boldsymbol{\rho}}$) for the base model, using equation (11), before adding low frequency components. The low frequency components of the background model are added using band-limited impedance module, BLIMP.

Figures (8 and 9) show inverted elastic parameters (**IP**-impedance, **IS**-impedance and $\boldsymbol{\rho}$) for the baseline and monitor models respectively, while figure (10) represents change in elastic parameters ($\mathbf{\Delta IP}$-impedance, $\mathbf{\Delta IS}$-impedance and $\mathbf{\Delta \rho}$), after adding low frequency component of well logs, as a result of inversion of total differences using equation (9).

Note that the actual elastic parameters estimated from well logs are also calculated and superimposed in bold dashed line. The inverted parameters are coinciding with actual parameters graphs.

Inverting for the base line, $\boldsymbol{m_0}$ and the time-lapse reflectivity model parameter changes ($\boldsymbol{\Delta m}$) requires that model parameters of monitor model $\boldsymbol{m_1}$ in equation (7) be re-written as:

$$\boldsymbol{m_1} = \boldsymbol{\Delta m} + \boldsymbol{m_0} \tag{12}$$

Substituting equation (12) into equation (7) yields

$$G_1\, (\boldsymbol{\Delta m} + \boldsymbol{m_0}\,) - G_0\, m_0 = \Delta d \tag{13}$$

By re-arranging the above equation, the inverse equation can be used to invert for base model parameter and the time-lapse change can be written as:

$$\mathbf{\Delta G}\boldsymbol{m_0} + \mathbf{G1}\ \boldsymbol{\Delta m} = \Delta\mathbf{d} \tag{14}$$

In augmented matrix notation, cost functions (3 and 4) are inverted to obtain the base line, $\mathbf{m_0}$, and the time-lapse reflectivity model parameter changes, $\mathbf{\Delta m}$ which can be written as:

$$J(\boldsymbol{m_0}, \mathbf{\Delta m}) = \left\| \begin{bmatrix} \Delta\mathbf{G} & \mathbf{0} \\ \mathbf{0} & \boldsymbol{G_1} \end{bmatrix} \begin{bmatrix} \boldsymbol{m_0} \\ \Delta\mathbf{m} \end{bmatrix} - \begin{bmatrix} \boldsymbol{d_0} \\ \boldsymbol{d_1} \end{bmatrix} \right\|^2 + \begin{bmatrix} \lambda^2 \boldsymbol{R_0^T R_0} & \mathbf{0} \\ \mathbf{0} & \lambda^2 \boldsymbol{R_1^T} R_1 \end{bmatrix} \begin{bmatrix} \boldsymbol{m_0} \\ \Delta\mathbf{m} \end{bmatrix} \tag{15}$$

Figures (11 and 12) show inverted elastic parameters (**IP**-impedance, **IS**-impedance and **ρ**) for the baseline and monitor models, while figure (13) represents change in elastic parameters (Δ(IP-impedance), Δ(IS-impedance) and Δρ) as a result of inversion of total differences using equation (14) after adding low frequency component of well logs. The resulting graphs form the time-lapse AVO inversions are in agreement with actual elastic parameters estimated from well logs.

Inversion of seismic differences data $(\boldsymbol{\Delta d})$only

Figures (14 and 15) show the difference of PP- and PS- data for the baseline and monitor models respectively. Note that seismic amplitudes of all seismic data sections are scaled to seismic amplitude of base line survey.

When $\mathbf{\Delta G} \approx \mathbf{0}$, the time-lapse inversion equations (9 and 14) of total inversion of differences given in previous section will be reduced and re-written as:

$$\mathbf{G_0}\ \boldsymbol{\Delta m} = \Delta\mathrm{d} \tag{16}$$

$$\mathbf{G_1}\ \boldsymbol{\Delta m} = \Delta\mathrm{d} \tag{17}$$

Thus, we are inverting for $\Delta\mathbf{m}$ using the difference of data $\mathbf{\Delta d}$. Time-lapse inversion of differences data only is a quick inverse scheme used to estimate the change in elastic model parameters. This method is based on assumption that if there is a change in time-lapse seismic data $\mathbf{\Delta d}$, this will yield a change in estimated $\Delta\mathbf{m}$. However, if there is no change in $\mathbf{\Delta d}$, then $\Delta\mathrm{m} = 0$ at a specific depth interval. The least-squares inversion equation for inverting of seismic difference only can be written as:

$$(G^T G + \lambda_1 W_m^T W_m)\Delta m = G^T \Delta\mathrm{d} \tag{18}$$

Figure (16) shows model parameter changes [$\Delta(\frac{\Delta\mathbf{I}}{\mathbf{I}})$, $\Delta(\frac{\Delta\mathbf{J}}{\mathbf{J}})$ and $\Delta(\frac{\Delta\boldsymbol{\rho}}{\boldsymbol{\rho}})$] from inverting time-lapse seismic data using equation (18) while figure (17) shows elastic model changes (Δ(IP), Δ(IS) and Δρ) after adding low frequency components of elastic model. Notice that the inverted elastic parameter changes are consistent with actual parameter changes as calculated from well logs.

In real time-lapse seismic data, it is almost impossible get seismic differences $\mathbf{\Delta d = 0}$ at specific depth interval. However, we would rather have very slight changes in amplitude that are not necessarily attributed to fluid property changes.

These very small changes in amplitudes in time-lapse seismic section can be attributed to geometry difference between time-lapse surveys or random noise or even processing differences. Therefore, a *cut-off* point can be set such that the seismic differences $\mathbf{\Delta d}$ fall below that *cut-off* point can then be set to zero. Thus, resulting differences data would be more representative of fluid change.

Sequential reflectivity-constrained inversion

In geophysical inversion, constraints can be included in inversion problem so as to refine estimated model parameters; thus producing more realistic inverted model. Geophysical constraints can be incorporated in either data space (Bube and Langan, 1997; Saeed et. al., 2010b) or in model spaces (Ajo-Franklin et. al., 2007; Saeed et al., 2010c) or in both space domains, which is often called blocky inversion (Claerbout, and Muir, 1973).

In the Pikes-Peak time-lapse seismic surveys, noise is noticeable and affects most of shot gathers of monitoring seismic survey, 2000, compared to baseline seismic survey, 1991. The source of noise is due to jack pumps that were operating during the course of seismic data acquisition. Therefore, In order to simulate the effect of jack pump noise in time-lapse model, small random noise of 0.1% were added to synthetic data of the base line (figures 18 and 19), while 1% of random noise were also added to monitoring model (Figures 20 and 21).

The *sequential reflectivity-constrained inversion* in equation (19) is one form of robust time-lapse inversion method whereby estimated model parameters of base survey are used to constrain inversion of monitoring model so as to ensure smooth variation in estimated elastic model parameters of monitoring model.

$$[(\boldsymbol{G^T G} + \boldsymbol{\lambda_1 W_m^T W_m} + \boldsymbol{\lambda_2 V^T V})]\boldsymbol{m_i} = \left[\boldsymbol{G^T d} + \boldsymbol{\lambda_2 V^T V}(\boldsymbol{m_{i-1}^M} - \boldsymbol{m_0^B})^T\right] \quad (19)$$

Where $\boldsymbol{V_{monit.}} = diag\left[abs\left(\boldsymbol{m_{i-1}^M} - \boldsymbol{m_0^B}\right)\right]$

Estimated model parameters of base model will act as prior information in inversion. Because $\boldsymbol{V}$ and $(\boldsymbol{m_{i-1}^M} - \boldsymbol{m_{i-1}^B})^T$ are functions of unknown base and monitor model parameters, this is a non-linear system, and iterative approach must be used. This is referred to iteratively re-weighted least squares, IRLS, (Wolke and Schwetlick, 1988).

We followed the approach of Farquharson and Oldenburg, (1998), by setting $\boldsymbol{V}$ and $(\boldsymbol{m_{i-1}^M} - \boldsymbol{m_{i-1}^B})^T = \boldsymbol{I}$ for the first iteration, which result in a traditional least-squares solution. The estimation of $\boldsymbol{m_i^B}$ for i=1 is then subsequently substituted again in equation (19) to obtain new $\boldsymbol{m_{i+1}^M}$. The procedure is repeated until the estimated model parameters of monitoring survey between successive IRLS iterations becomes less than tolerance value, τ given in convergence limit equation (20).

$$\frac{\|\mathbf{m}^{i+1}-\mathbf{m}^{i}\|_2}{1+\|\mathbf{m}^{i+1}\|_2} < \tau \qquad (20)$$

Figure (22) shows that inverted acoustic impedances for the monitoring model using reflectivity-constrained inverse scheme is matching actual impedances fairly well in the presence of noise. Figure (23) shows regularization parameter during the inversion while RMS error during inversion (figure 24) shows converging of the program towards final solution.

In order to test stability of inversion algorithm and reliability of resulting elastic parameters in the presence of high percentage of noise, random noise of a magnitude that 10 times size of monitoring data is used in this test. Figure (25) shows elastic impedances of monitoring model after inversion. As expected, P-impedance is less affected by noise, while S-impedance and density are influenced by noise. This experiment can assist in deciding which reflectivity attribute to be constrained more as well as the percentage of reflectivity attribute of base survey to be used to constrain inverting model parameters of monitor model.

CONCLUSIONS

The application of three different inverse schemes for time-lapse AVO inversion is presented in this report. Obtained elastic impedances from inverse schemes are in very good agreement with actual elastic impedances calculated from well logs. The developed codes were optimized to perform inversion in less time, and shows fast convergence with less number of iterations for robust time-lapse AVO inversion. Results from inverting noise data can assist in choosing appropriate reflectivity attributes of base model to be used in constraining inversion of monitor survey.

ACKNOWLEDGEMENTS

The authors wish to thank all of CREWES sponsors for supporting this study.

REFERENCES

Ajo-Franklin, J.B., Minsley B.J. and Daley T.M., 2007, Applying compactness constraints to differential traveltime tomography. Geophysics, **72**, 67-75.

Bube, K.P., and Langan, R.T., 1997, Hybrid lambda1/lambda2 minimization with application to tomography: Geophysics, **62**, 1183-1195.

Claerbout, J.F. and Muir, F., 1973, Robust modeling with erratic data: Geophysics, **38**, 826-844.

Constable, S.C., Parker, R.L., and Constable, C.G., 1987, Occam's inversion: A practical algorithm for generating smooth models from electromagnetic sounding data: Geophysics, **52**, 289-300.

Farquharson, C. G., and Oldenburg, D.W., 1998, Non-linear inversion using general measures of data misfit and model structure: Geophy. J. Int., **134**, 213-227.

Ferguson, R. J., Margrave G.F., 1996, A simple algorithm for band-pass impedance inversion, CREWES Research Report, 8, 1-10.

LandrØ, M., 2001, Discrimination between pressure and fluid saturation changes from time-lapse seismic data: Geophysics, 66, 836-844.

Saeed, A.N., Lines, L.R., and Margrave, G.F., 2010a, Time-lapse AVO inversion: model building and AVA analysis: CREWES report, **22**.

Saeed, A.N., Lines, L.R., and Margrave, G.F., 2010b, Iteratively re-weighted least squares inversion for the estimation of density from well logs: part one: CREWES report, **22**.

Saeed, A.N., Lines, L.R., and Margrave, G.F., 2010c, Iteratively re-weighted least squares inversion for the estimation of density from well logs: part two: CREWES report, **22**.

Wolke, R., and Schwetlick, H., 1988, Iteratively re-weighted least squares algorithms, convergence analysis, and numerical comparisons: SIAM Journal of Scientific and statistical computation, **9**, 907-921.

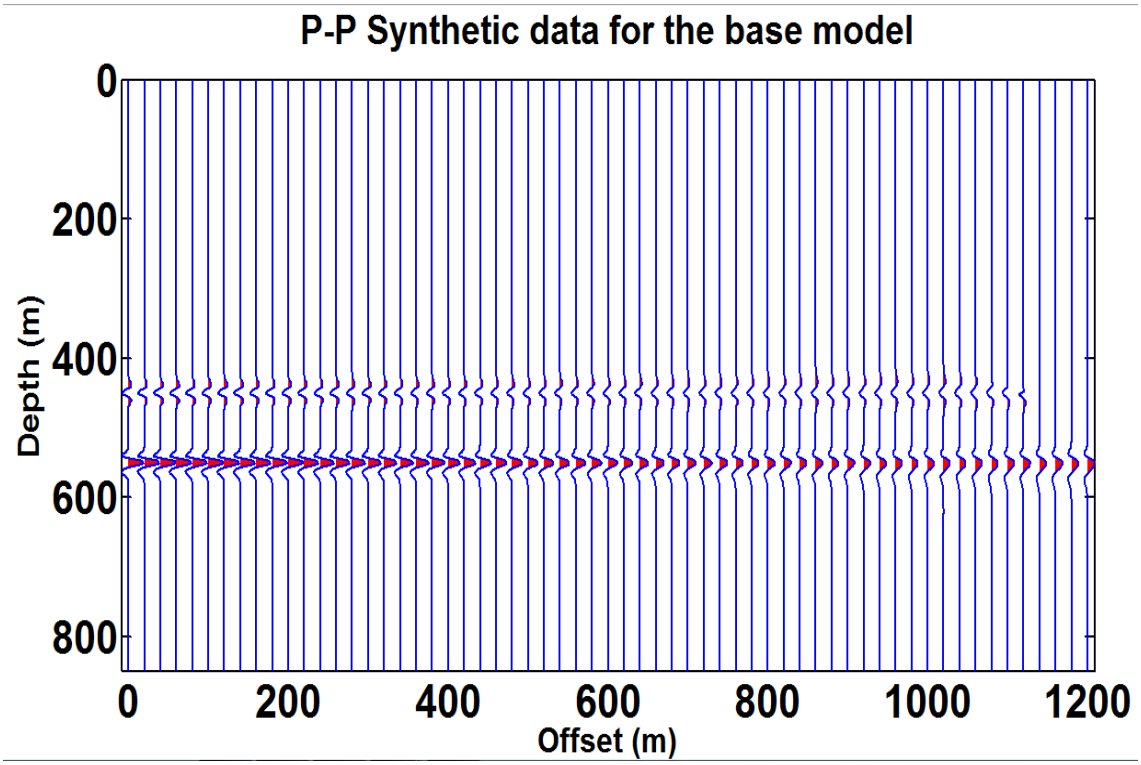

FIG.1. **P-P** synthetic seismic data for the **baseline** model of the Pikes Peak time-lapse model.

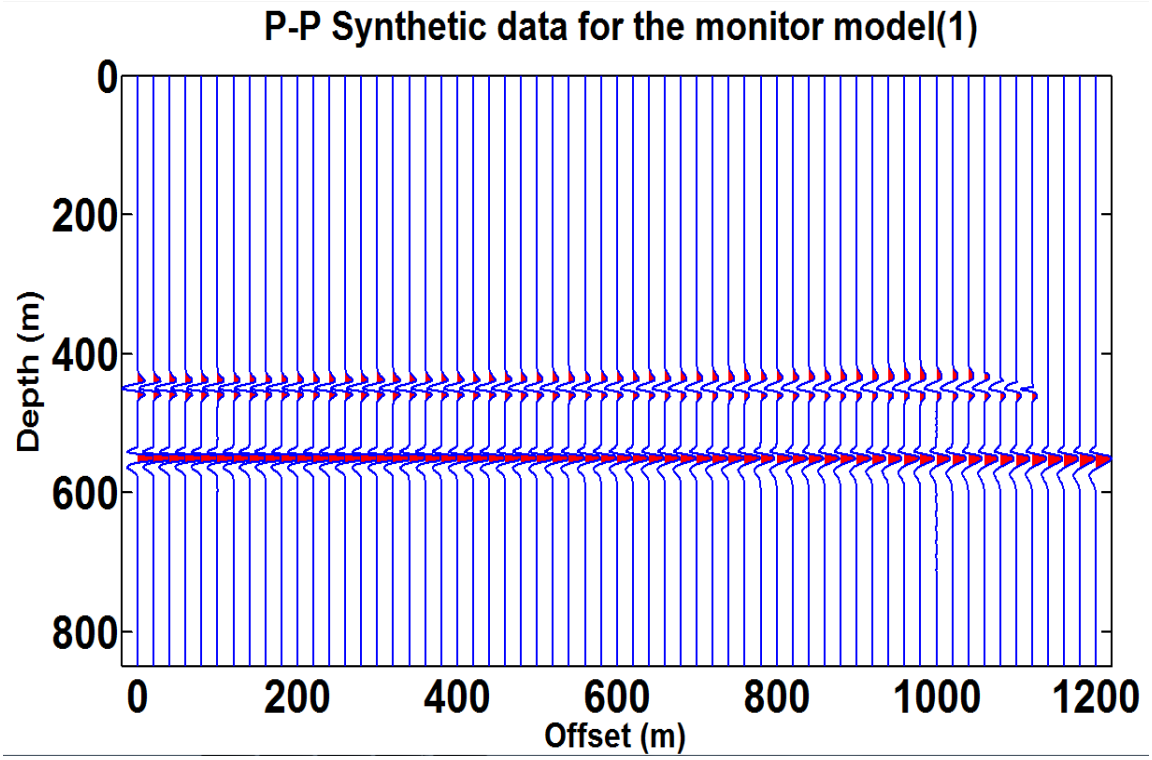

FIG.2. **P-P** synthetic seismic data for the **monitor** model of the Pikes Peak time-lapse model.

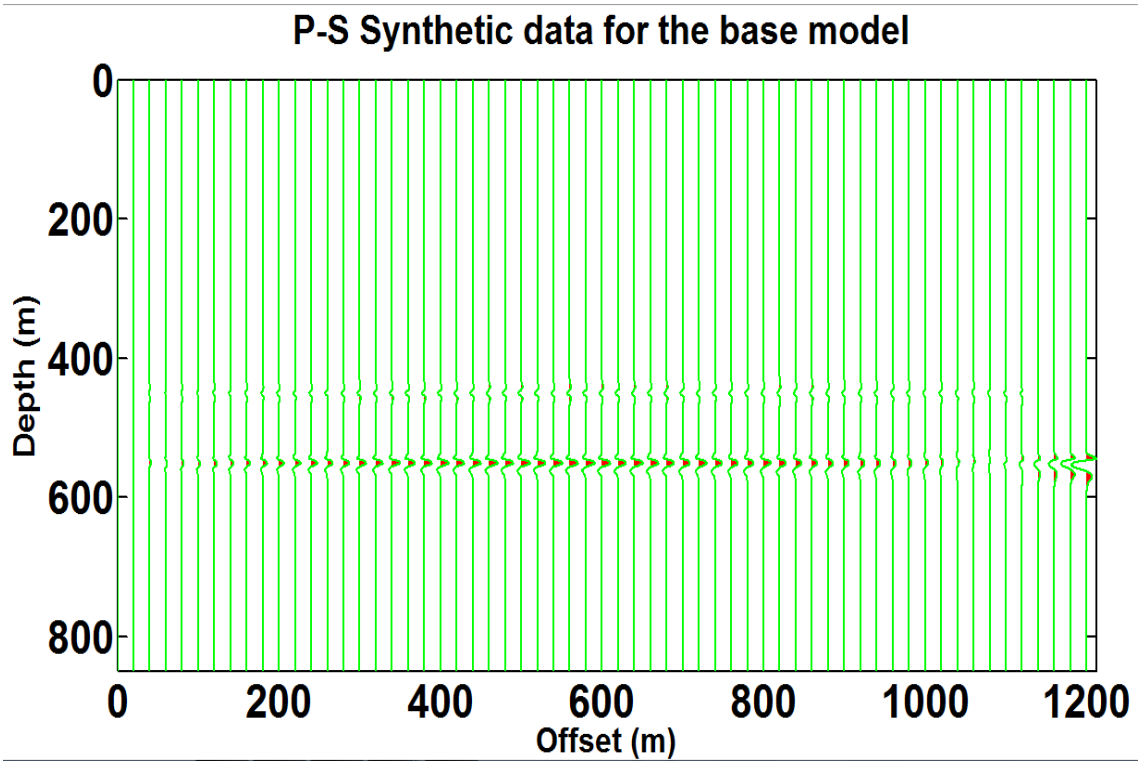

FIG.3. **P-S** synthetic seismic data for the **baseline** model of the Pikes Peak time-lapse model.

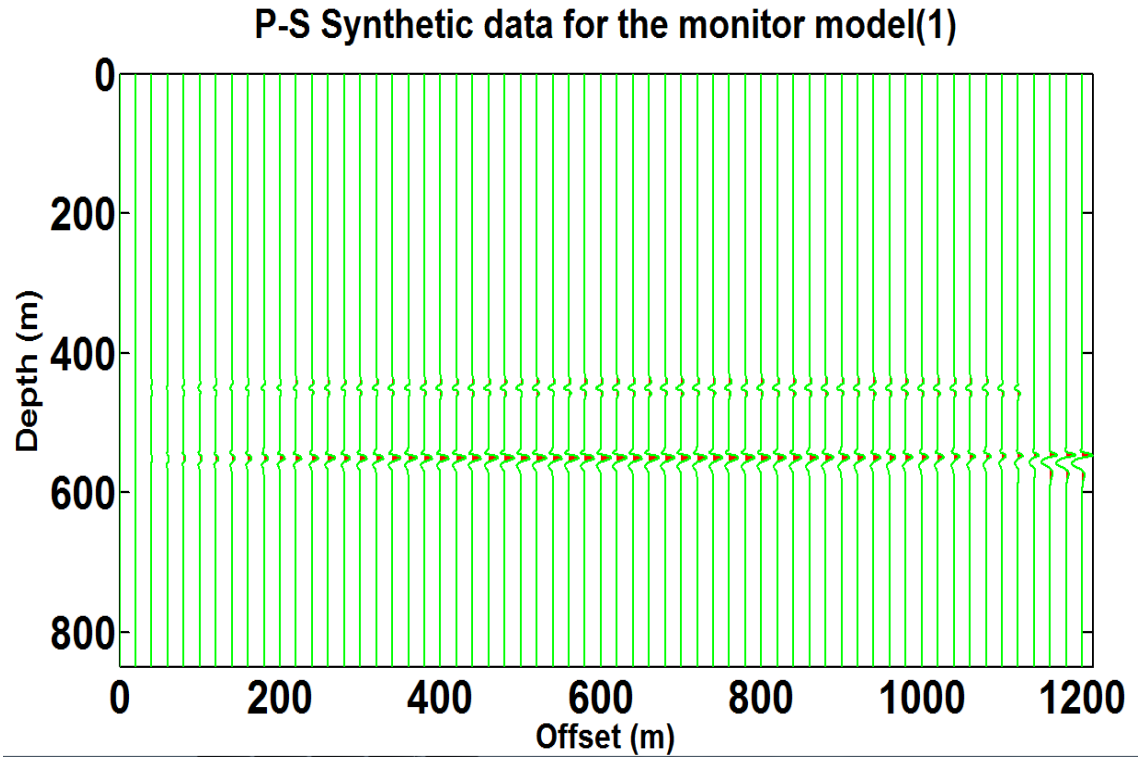

FIG.4. **P-S** synthetic seismic data for the **monitor** model of the Pikes Peak time-lapse model.

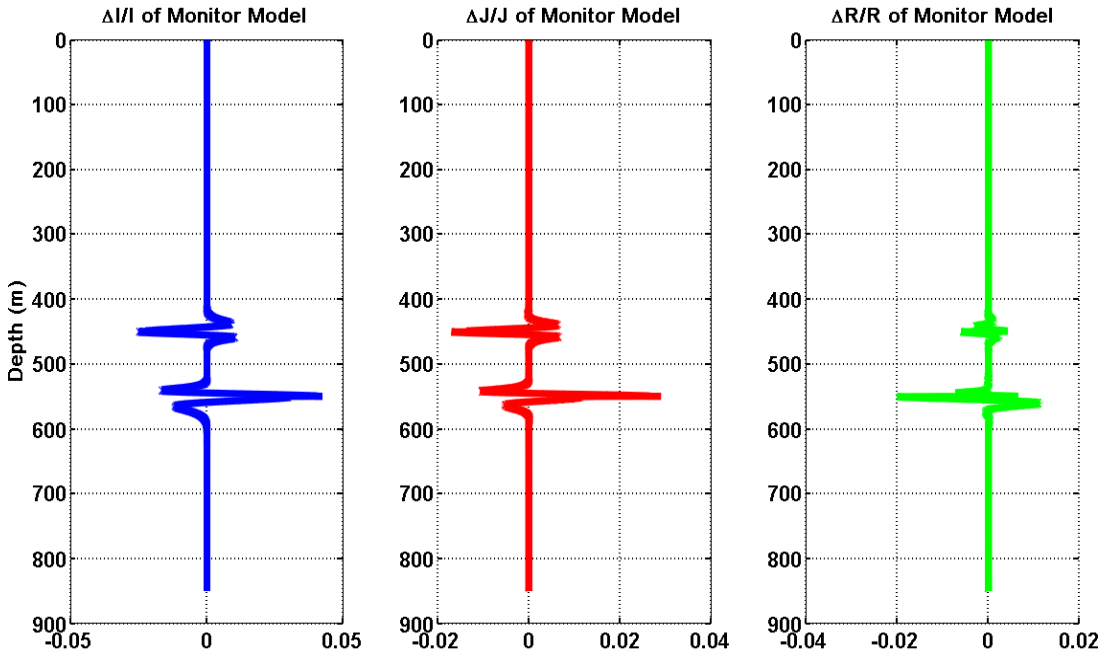

FIG.5 Estimated model parameters ($\frac{\Delta I}{I}$, $\frac{\Delta J}{J}$ and $\frac{\Delta R}{R}$) for the monitor model before adding low-frequency of logs.

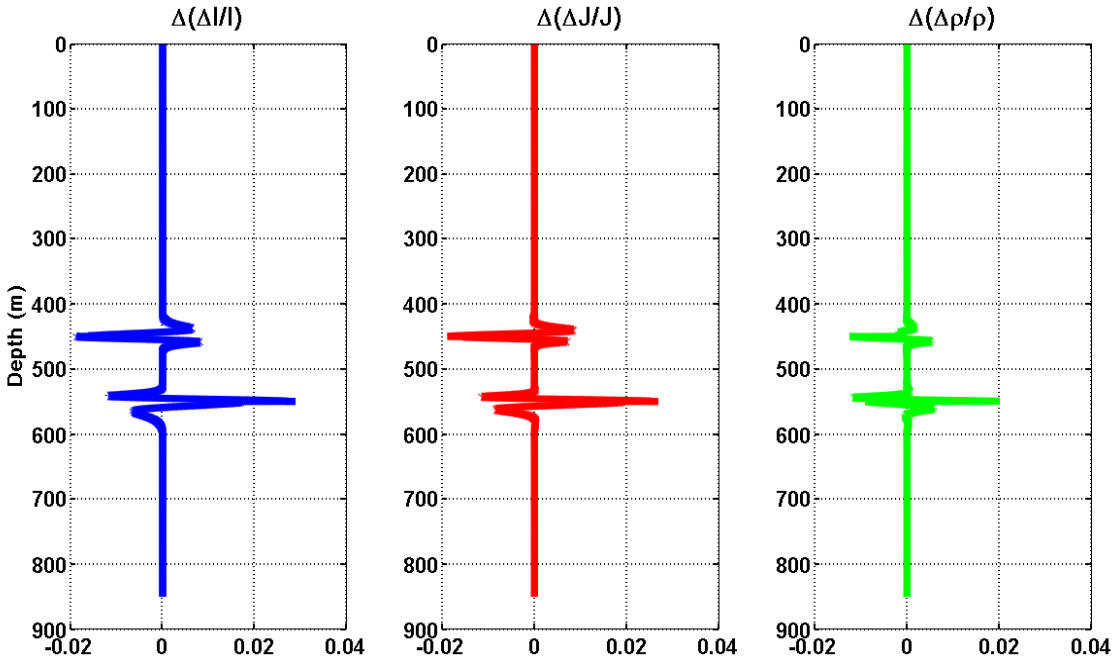

FIG.6 Estimated model parameters changes [$\Delta(\frac{\Delta I}{I})$, $\Delta(\frac{\Delta J}{J})$ and $\Delta(\frac{\Delta R}{R})$] for the time- lapse model before adding low-frequency of logs.

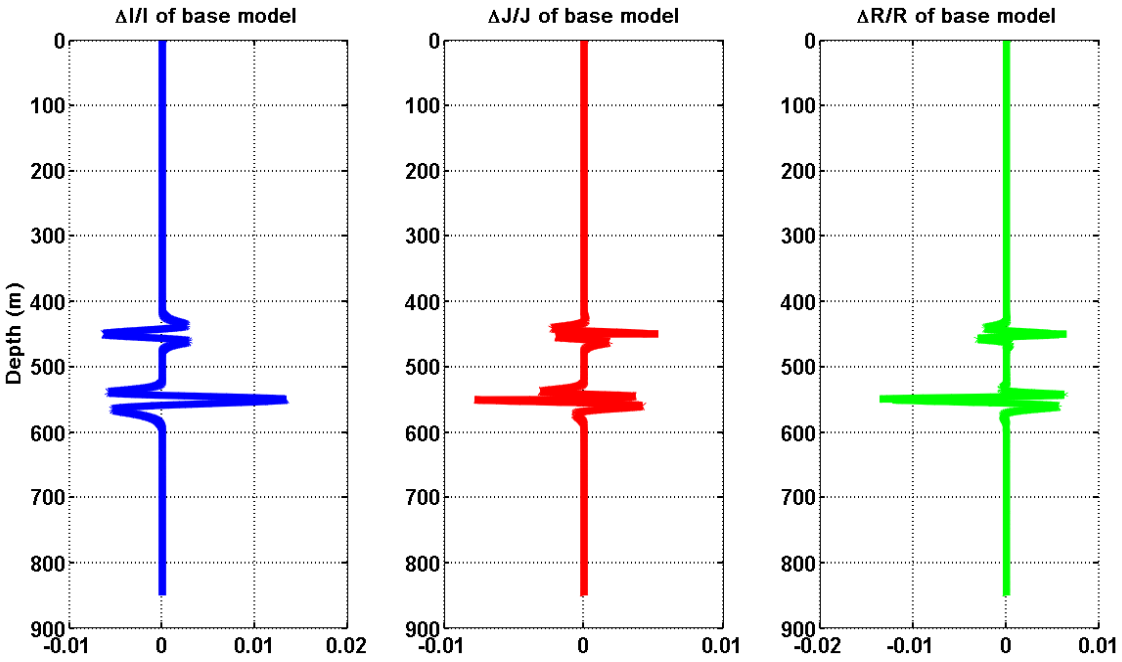

FIG.7 Estimated model parameters ($\frac{\Delta I}{I}$, $\frac{\Delta J}{J}$ and $\frac{\Delta R}{R}$) for the base model before adding low-frequency of logs.

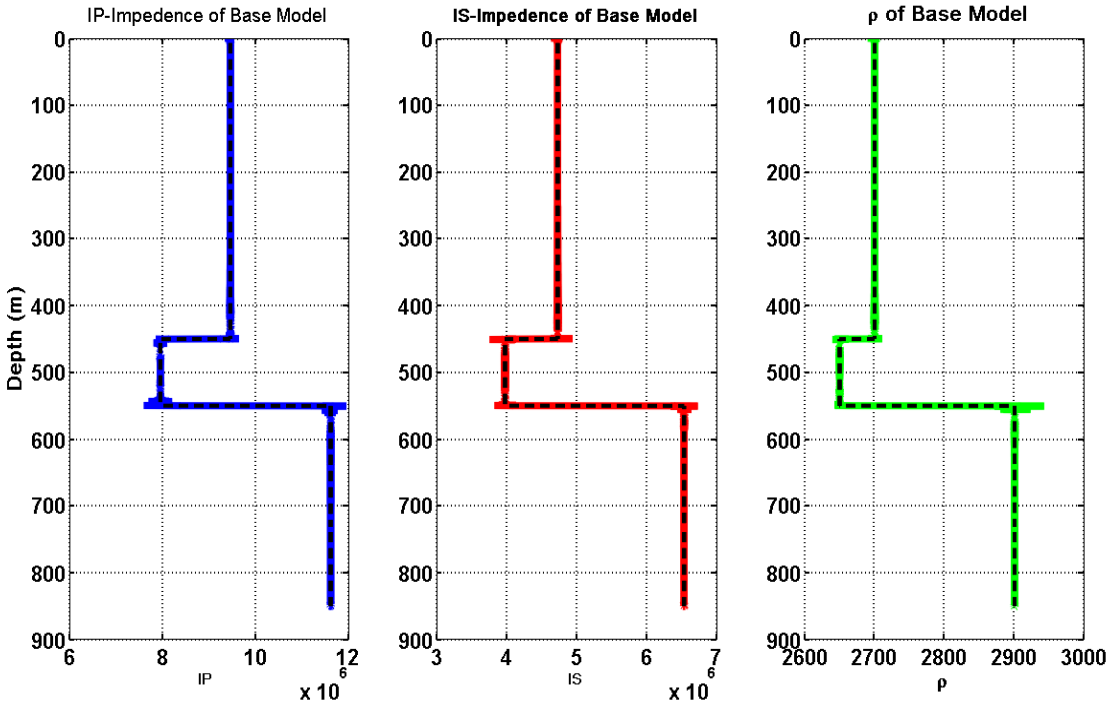

FIG.8 Elastic parameters (IP, IS and ρ) of the base model after adding low frequency. Embedded graphs in bold black dotted lines represent actual (IP, IS and ρ) calculated from logs.

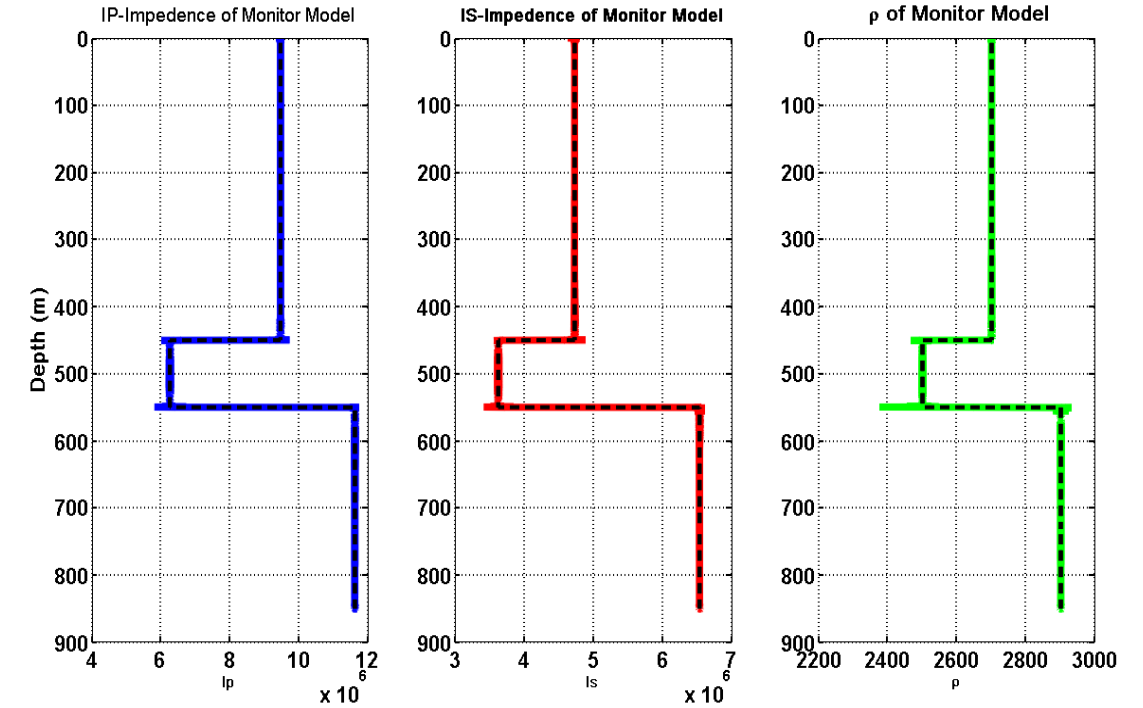

FIG.9 Elastic parameters (IP, IS and ρ) of the monitor model after adding low frequency. Embedded graphs in bold black dotted lines represent actual (IP, IS and ρ) calculated from logs.

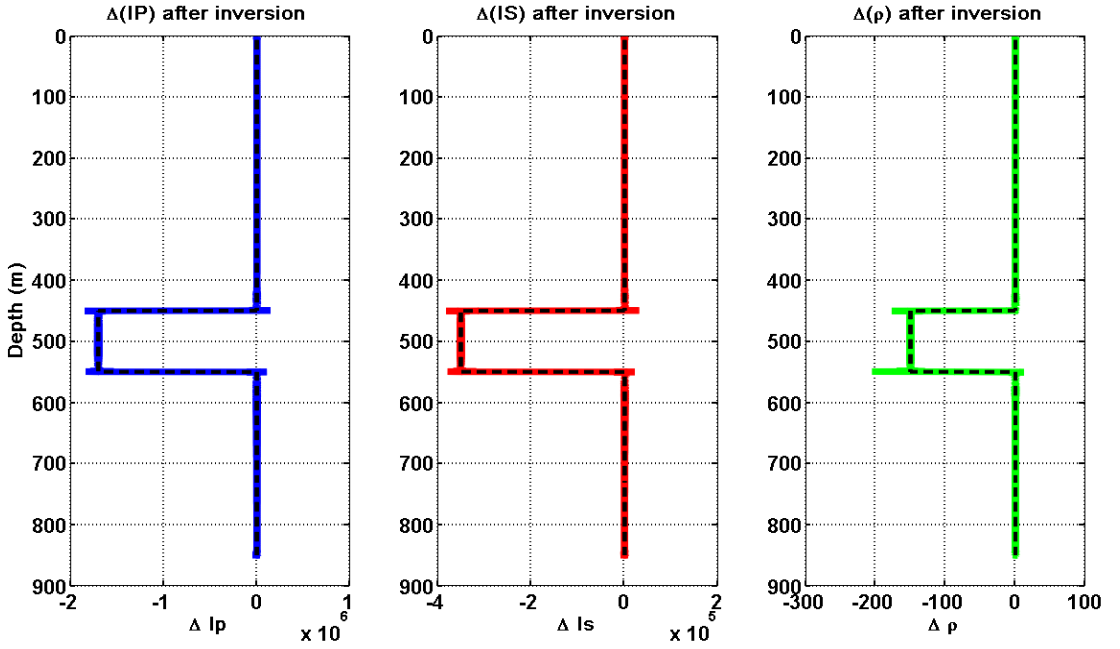

FIG.10 Elastic parameter changes (ΔIP, ΔIS and Δρ) of the time-lapse model after adding low frequency. Embedded graphs in bold black dotted lines represent actual elastic parameter changes calculated from logs.

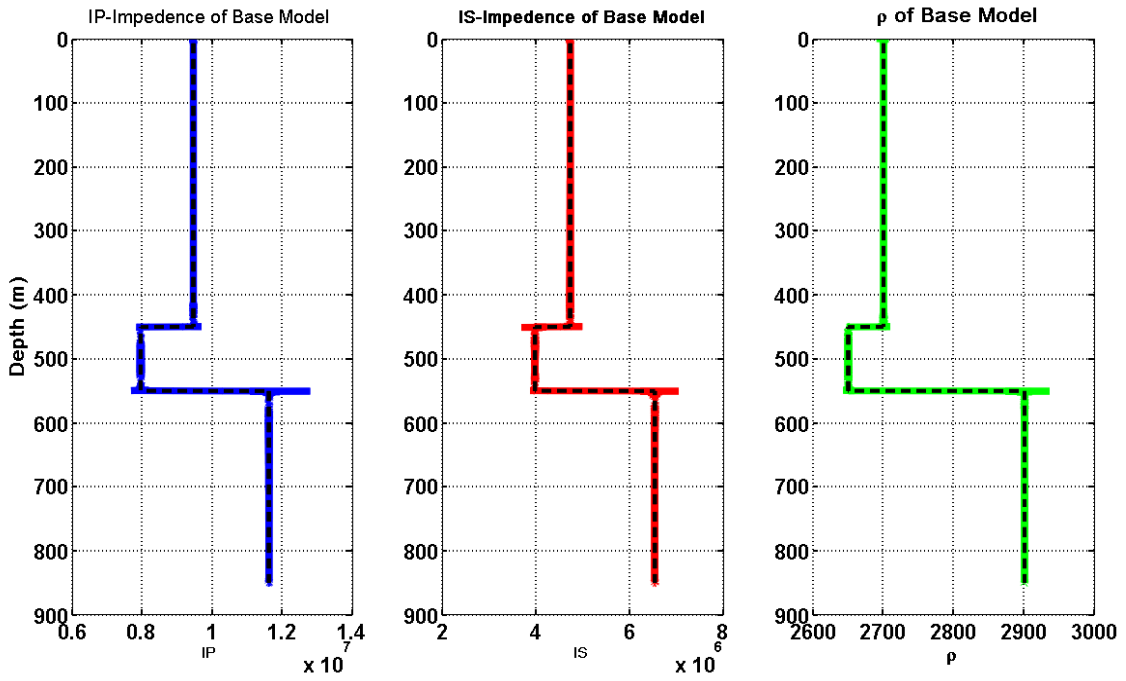

FIG.11. Elastic parameters (IP, IS and ρ) of the base model using equation (14) after adding low frequency. Embedded graphs in bold black dotted lines represent actual (IP, IS and ρ) calculated from logs.

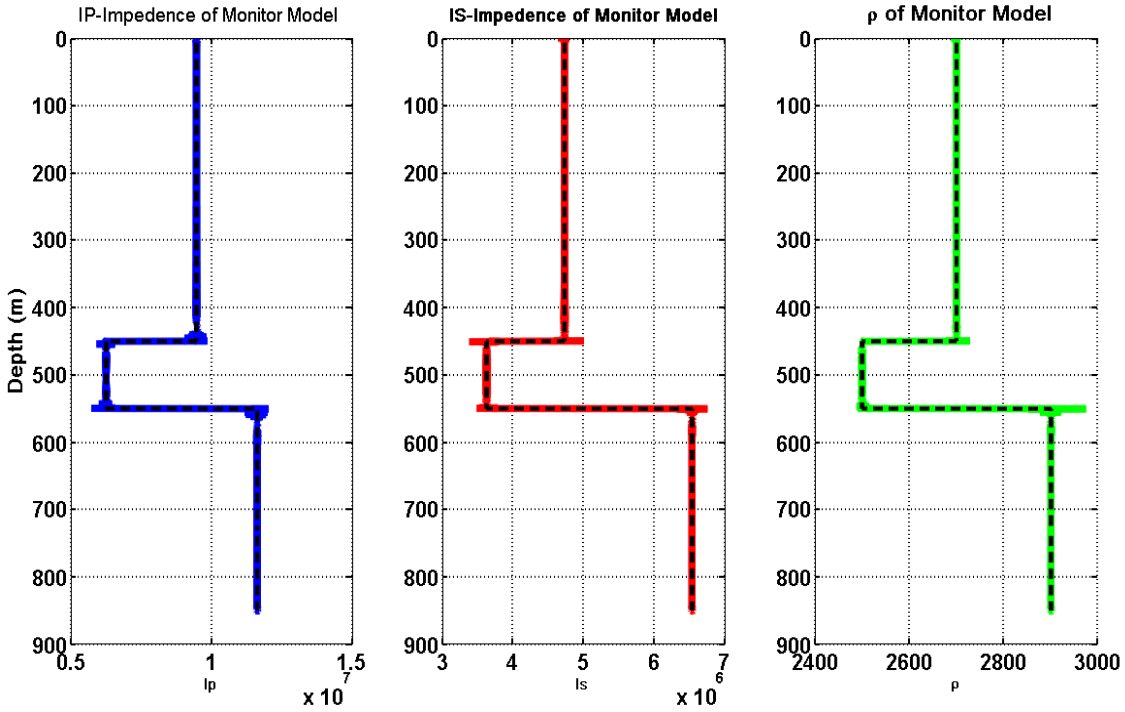

FIG.12. Elastic parameters (IP, IS and ρ) of the monitor model using equation (14) after adding low frequency. Graphs in bold black dotted lines represent actual (IP, IS and ρ) from logs.

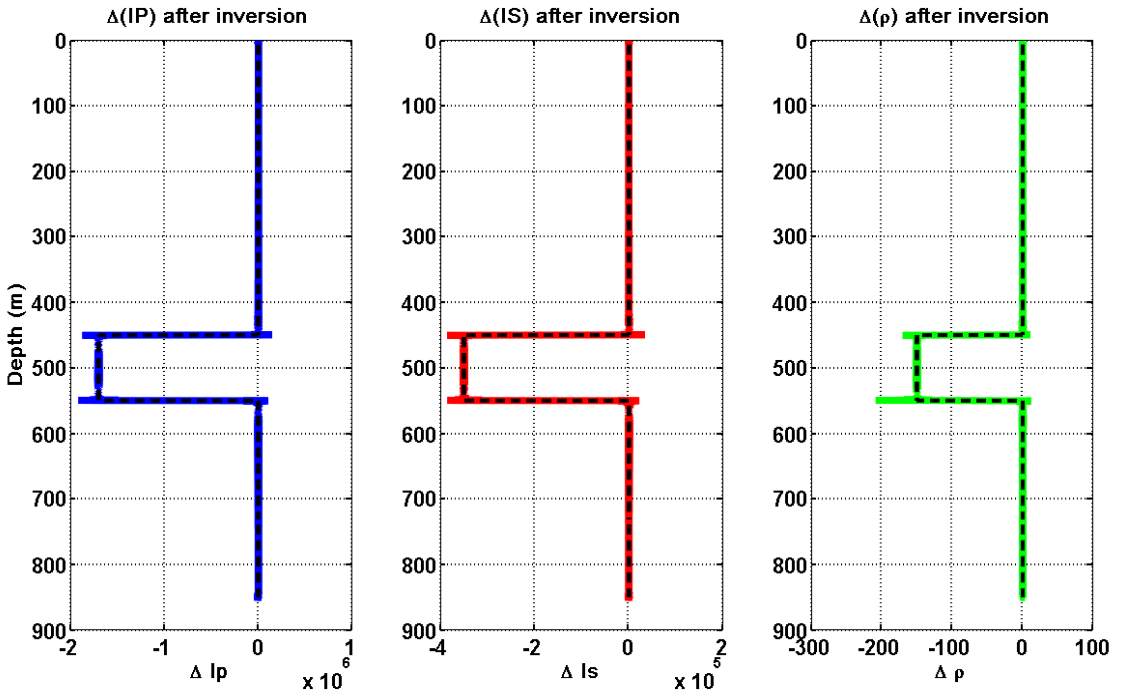

FIG.13 Elastic parameter changes (ΔIP, ΔIS and Δρ) of the time-lapse model using equation (14) after adding low frequency. Embedded graphs in bold black dotted lines represent actual elastic parameter changes calculated from logs.

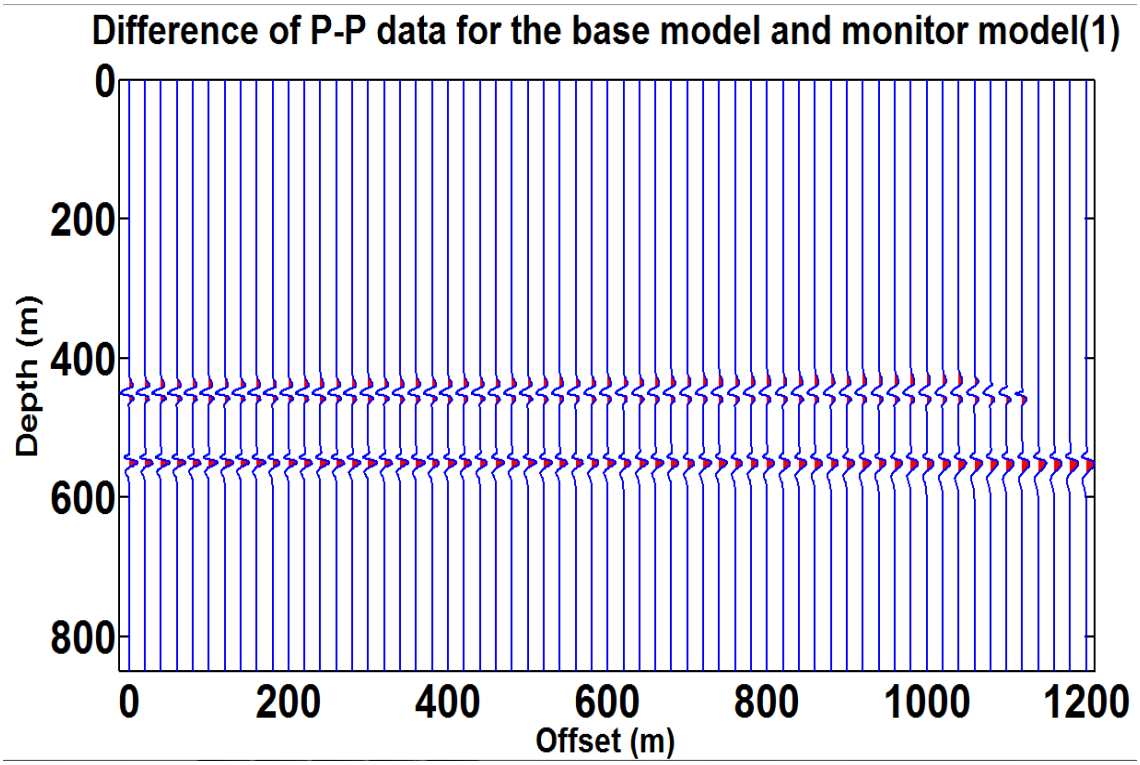

FIG.14. Difference of P-P synthetic seismic data for the baseline and monitor models of the Pikes Peak time-lapse model.

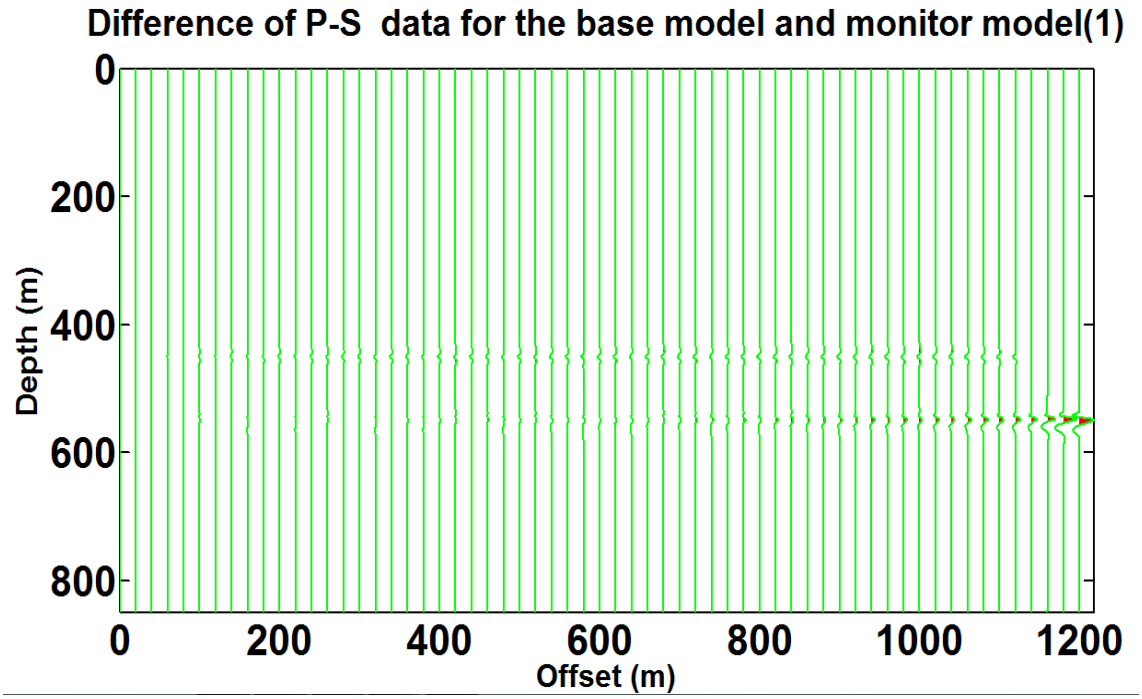

FIG.15. Difference of P-S synthetic seismic data for the baseline and monitor models of the Pikes Peak time-lapse model.

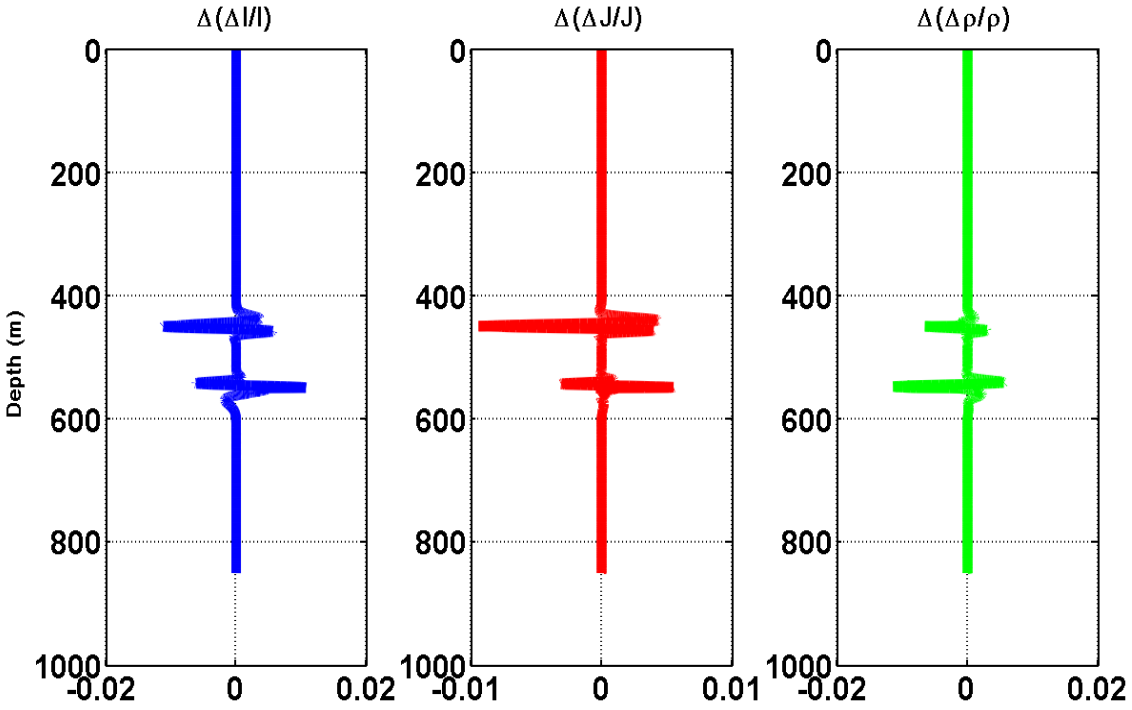

FIG.16 Estimated model parameters changes [$\Delta(\frac{\Delta I}{I})$, $\Delta(\frac{\Delta J}{J})$ and $\Delta(\frac{\Delta R}{R})$] from inversion of data differences only before adding low-frequency of logs.

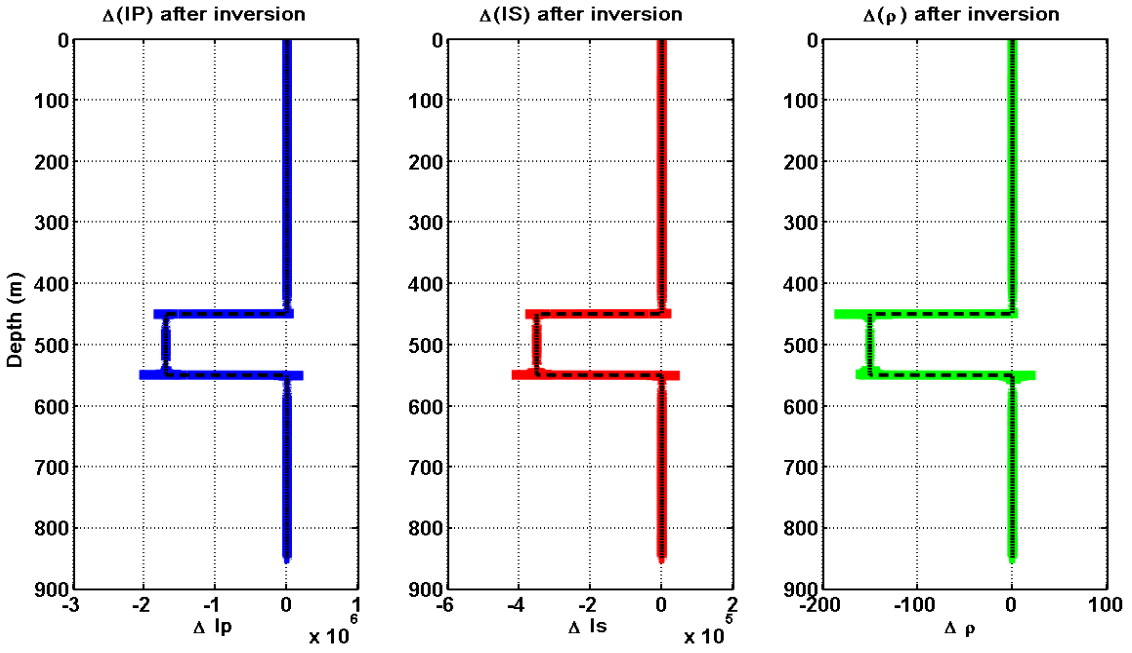

FIG.17 Elastic parameter changes (ΔIP, ΔIS and Δρ) of the time-lapse model from inversion of data differences only after adding low frequency. Embedded graphs in bold black dotted lines represent actual elastic parameter changes calculated from logs.

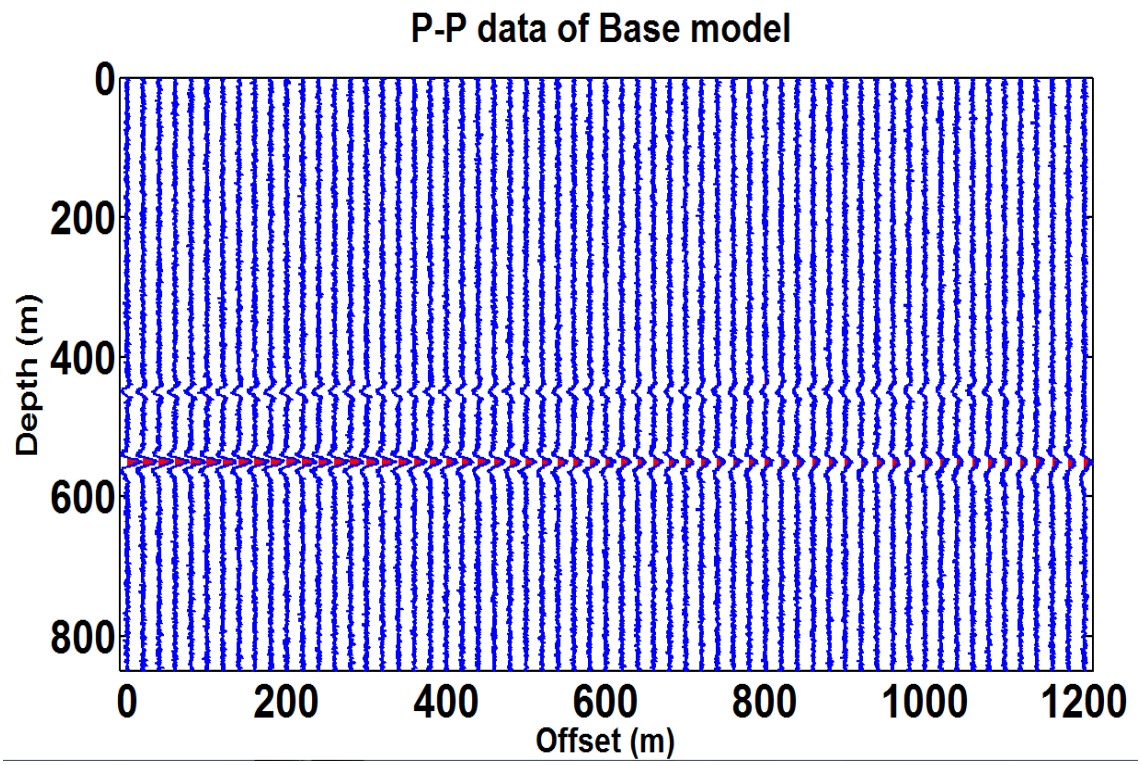

FIG.18. **P-P** synthetic seismic data for the **base** model with **0.001** random noise added.

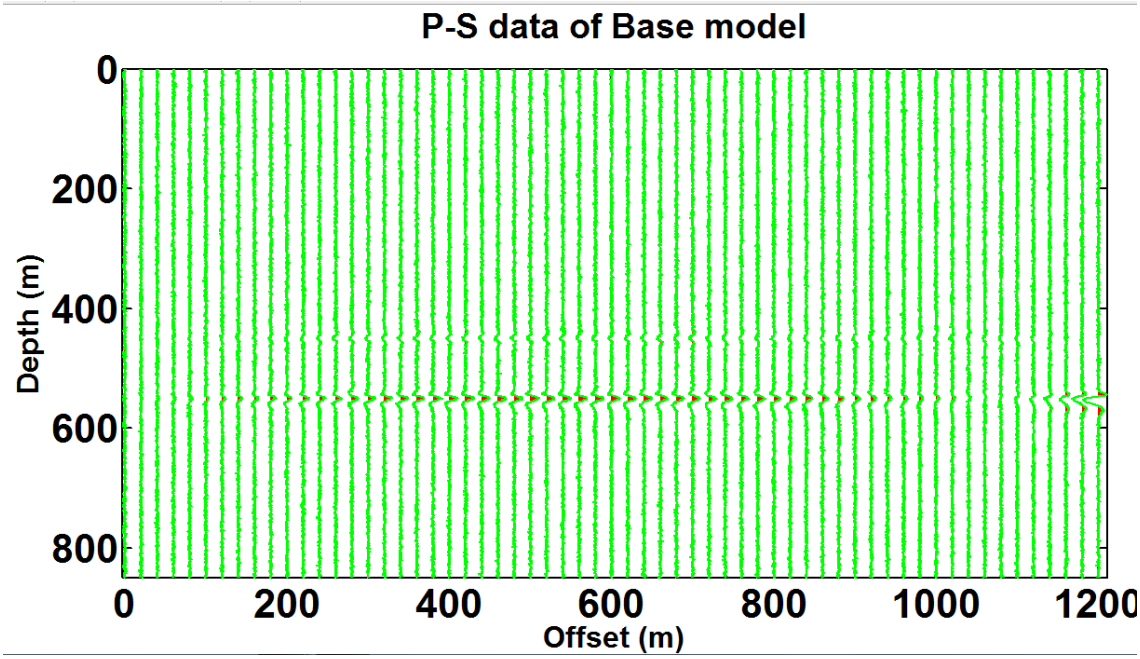

FIG.19. **P-S** synthetic seismic data for the **base** model with **0.001** random noise added.

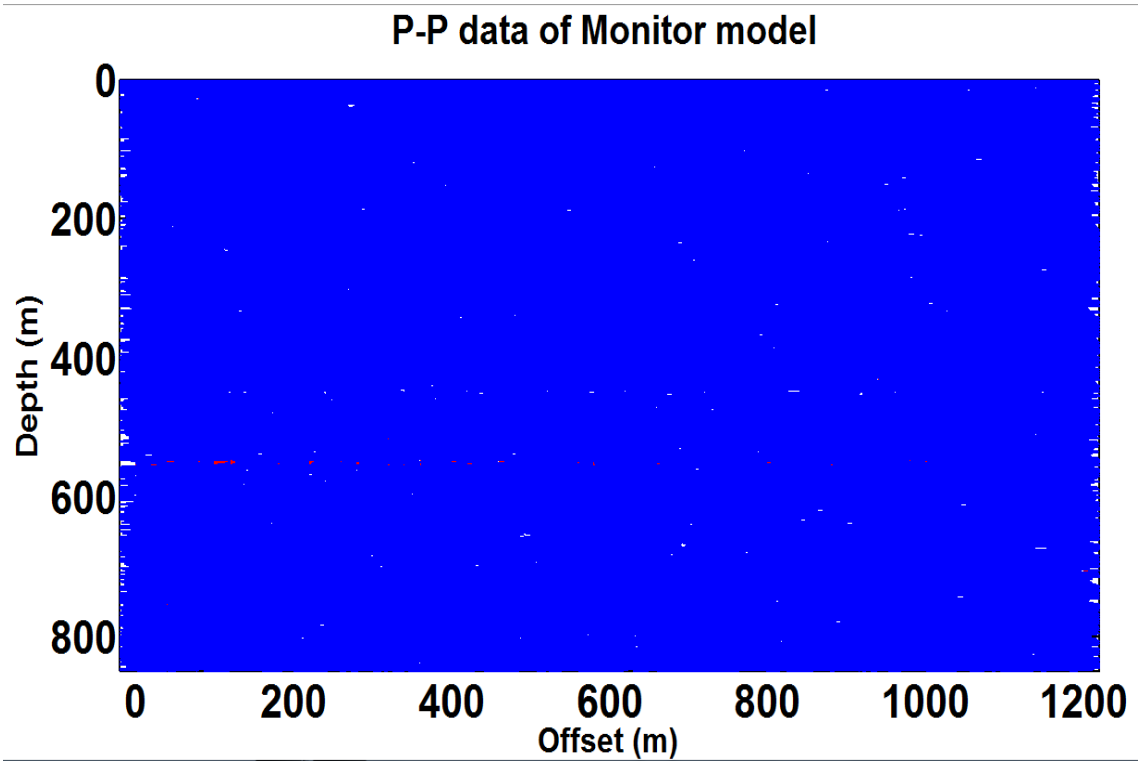

FIG.20. **P-P** synthetic seismic data for the **monitor** model with **0.1** random noise added.

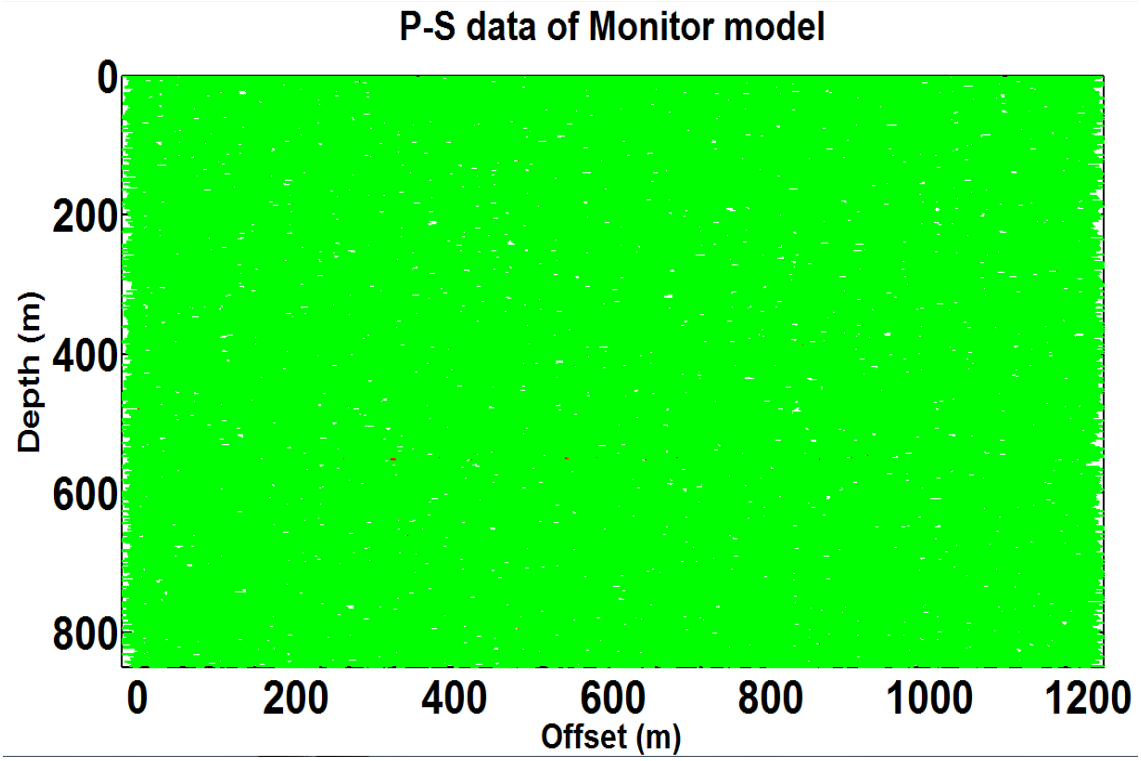

FIG.21. **P-S** synthetic seismic data for the **monitor** model with **0.1** random noise added.

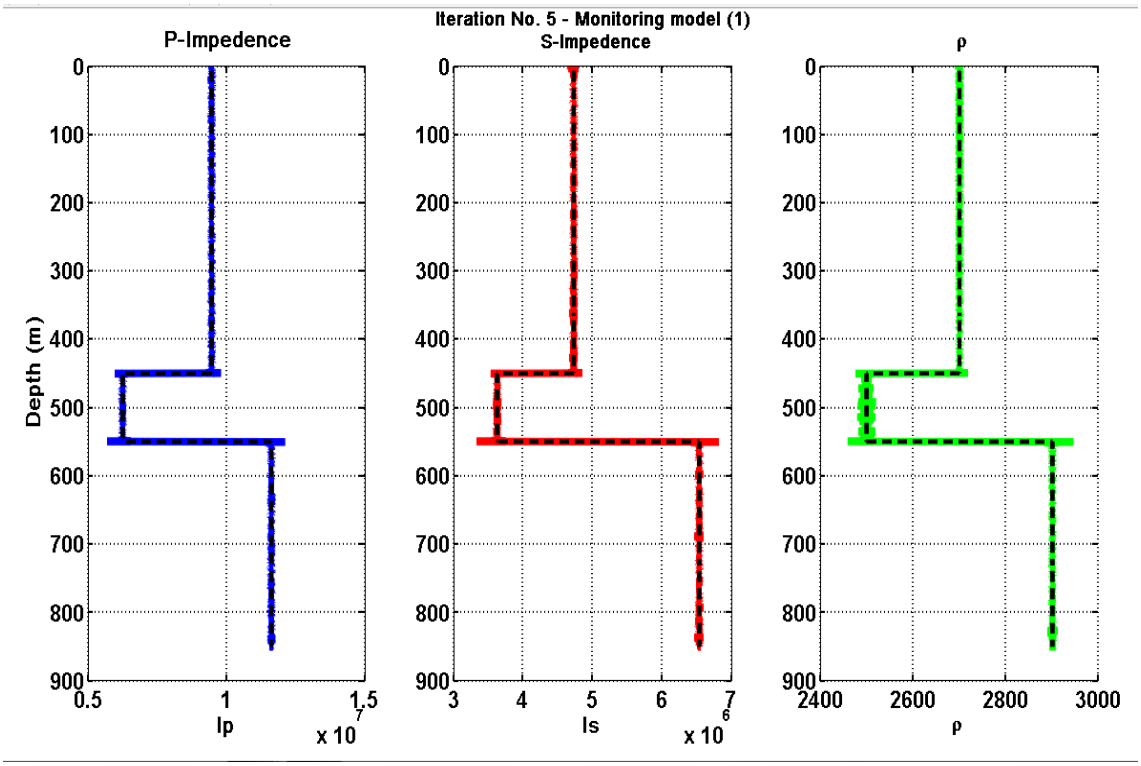

FIG.22. Elastic parameters (IP, IS and ρ) using sequential reflectivity-constrained inversion of the noisy (0.01) monitor model after adding low frequency.

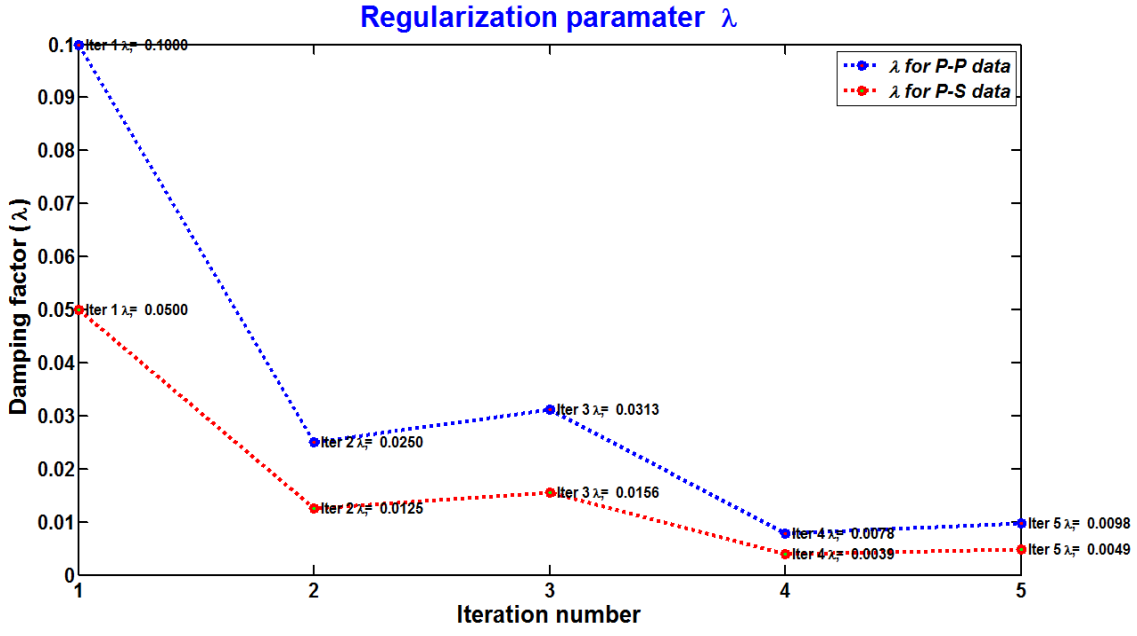

FIG.23. Regularization parameter during reflectivity-constrained Inversion.

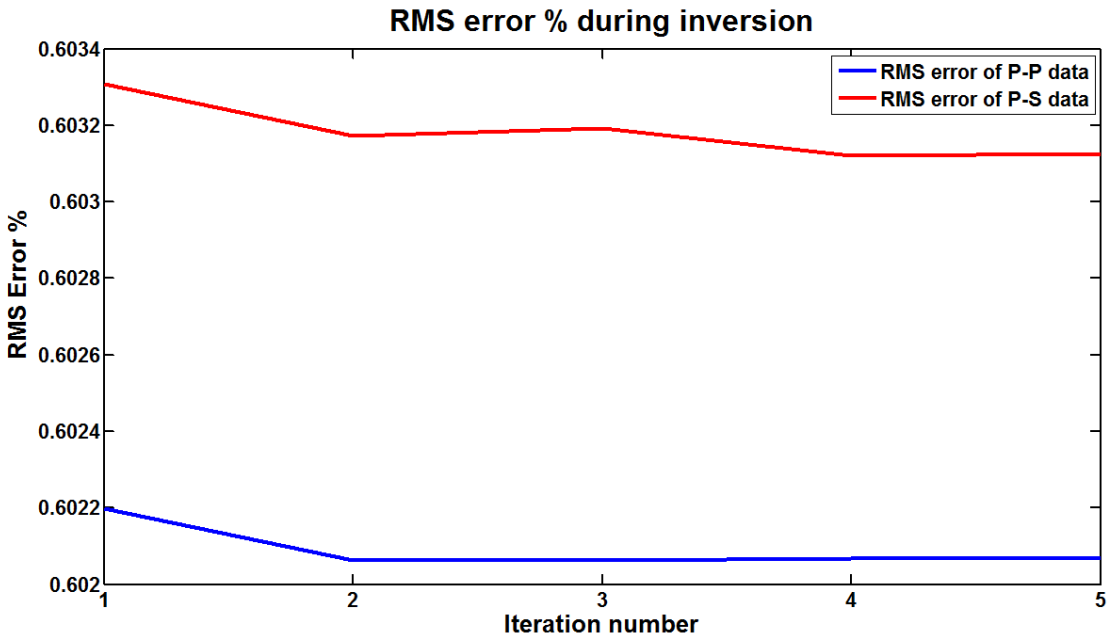

FIG.24. RMS error during reflectivity- constrained Inversion scheme.

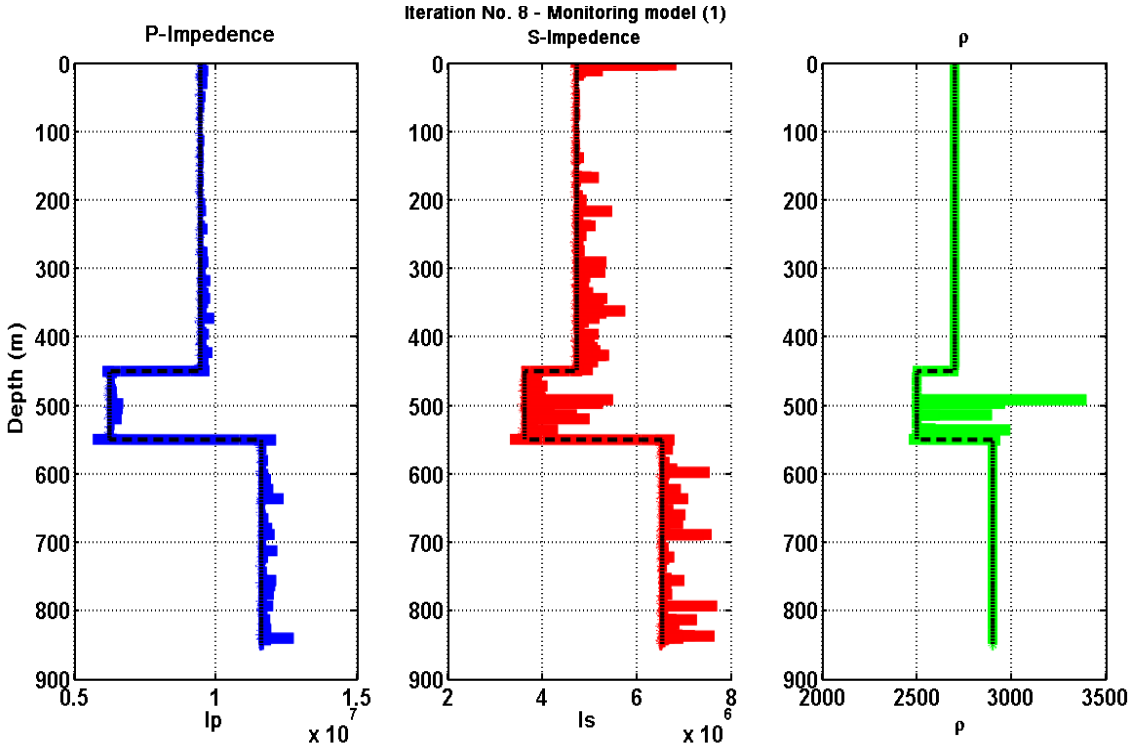

FIG.25. Elastic parameters (IP, IS and ρ) using sequential reflectivity-constrained inversion of the noisy (10 times amount of noise in figure 22) monitor model after adding low frequency.